Available online at www.sciencedirect.com
SCIENCE DIRECT®
Journal of Nuclear Materials 340 (2005) 271–283
journal of nuclear materials
www.elsevier.com/locate/jnucmat

Influence of Pt, Fe/Ni/Cr-containing intermetallics and deuterium on the oxidation of Zr-based materials

Clara Anghel [a,*], Gunnar Hultquist [a], Magnus Limbäck [b]

[a] Division of Corrosion Science, Department of Materials Science and Engineering, Royal Institute of Technology, Drottning Kristinas väg 51, S-100 44 Stockholm, Sweden
[b] Westinghouse Electric Sweden AB, S-721 63 Västerås, Sweden

Received 15 October 2004; accepted 22 December 2004

Abstract

An in situ gas phase analysis technique and the ^{18}O-SIMS technique are used to evaluate the transport of oxygen and hydrogen in oxidation of Zr-based materials. At 400 °C, it is found that oxygen dissociation efficiency decreases in the order: Pt > Zr_2Fe > Zr_2Ni > $ZrCr_2$ ⩾ Zircaloy-2. Two Zr-plates partly coated with 200 Å porous Pt, with and respectively without D in the substrate, were oxidized in two stages at 400 °C. SIMS depth profiles in the Pt area show that an enhanced oxidation takes place mainly by inward oxygen transport. A minimum in the oxide thickness was found near the Pt area on both Zr plates. Two Ar-filled Zircaloy-2 tubes with ZrSn liner were exposed at 370 °C to 22 mbar water, filled in from one side. Our experimental results suggest that a proper choice of the SPP composition and size distribution can lead to reduced hydrogen uptake during oxidation of Zr-based materials in water.

1. Introduction

The corrosion behaviour of Zr-based materials has been extensively studied during the last decade with a wide variety of techniques [1–10]. The role of a surface oxide layer is to protect the metal substrate against the corrosive environment. A protective metal oxide should be gas-tight and therefore only ions should be transported in the oxide. This situation is often assumed but rarely (if ever) confirmed. It is generally considered that in the oxidation of the Zr-based materials, the oxide is growing mainly by inward oxygen transport [1,4,5]. One possible factor related to the transport of molecules is the existence of pores inside the oxide. It was found that the zirconium oxide layer is porous not only in the outer part, but also within the barrier layer [8,11]. The distribution of ZrO_2 phases in the oxide layer is also changing in depth. Tetragonal and monoclinic ZrO_2 phases have been reported [3,6,8,12]. The fraction of tetragonal phase is higher at the oxide/metal, O/M, interface (stabilized by high compressive stress) and is irregularly distributed in the oxide [3]. The tetragonal to monoclinic phase transformation takes place as a result of stress relief with a volume expansion of 7% and generates defects like cracks and pores (easy diffusion pathways) [3]. This transformation can occur inside the barrier layer, possibly inducing porosity within the

* Corresponding author. Tel.: +46 8 7906670; fax: +46 8 208284.
E-mail address: anghel@kth.se (C. Anghel).

0022-3115/$ - see front matter © 2005 Elsevier B.V. All rights reserved.
doi:10.1016/j.jnucmat.2004.12.005

barrier layer [8]. The porosity development in the zirconium oxide scale is considered to be a main reason that leads to the transition from parabolic to linear oxide growth kinetics [5]. Zhilyaev and Szpunar [12] proposed a model for oxygen diffusion through the oxide scale considering stress development.

Enhanced oxidation of Zr-based materials in atomic oxygen enriched gas obtained by microwave discharge has been reported in the literature [9,10]. This shows that increased availability of dissociated oxygen at the oxide/gas, O/G, interface generates enhanced oxidation. Raspopov and co-workers [9] suggested that oxygen chemisorption is likely to be a rate-limiting step for the oxidation process at the early stages of oxidation. To understand how the dissociation rate of oxygen influences Zr oxidation at the temperatures relevant for the nuclear industry, we have to consider in which form oxygen is transported through the oxide layer. For oxygen dissociation to take place an activation energy has to be overcome. At 300–400 °C, the thermal energy is low for oxygen dissociation on ZrO_2 but Pt and second-phase particles, SPP, may catalyze the dissociation. The presence of SPP incorporated, partly un-oxidized, in the oxide layer may therefore influence the ratio between molecular and dissociated oxygen transport across the oxide. One aim with this paper is to study O_2 dissociation rates on Zr-based materials and their possible influence on the corrosion rate. The dissociation of O_2 on Pt, pre-oxidized Zircaloy-2 and pre-oxidized Fe/Ni/Cr containing intermetallics has been measured and will be discussed in this paper. Also the influence of Pt, a very effective oxygen dissociating element, ODE, on the oxidation of Zr is presented here.

Isotope monitoring techniques have been used to investigate the mechanism of oxygen and hydrogen incorporation in the growing zirconia layer and substrate [11,13–15]. Many studies related to the influence of hydrogen on Zr oxidation have been published lately [3,6,8,11,16,17]. Recent publications dealing with other metals than Zr [16,18,19] have concluded that the presence of hydrogen in the metal substrate or in the gas phase has an effect on oxidation by increasing the metal outward transport, which eventually can generate voids at the metal/oxide interface. One possible mechanism is based on a proton-induced high concentration of metal ion vacancies in the oxide, which is likely to result in an increased metal ion transport [19]. Oxidation of Zr by cation outward diffusion via cation vacancies was already taken into consideration in early 50s by Gulbransen and Andrew [1]. The Zr-metal and oxygen mobilities during oxidation of Zircaloy-4 at 633 K in water and in dry O_2 were investigated by Grandjean and Serruys [20] using Xenon marker atoms implanted into the preformed oxide and the Rutherford backscattering spectrometry (RBS) technique. They interpreted their results that, before transition, the oxide grows only by oxygen inward transport, both in water and in oxygen exposures. However in their experiments performed in water, big losses of Xenon occurred, in contrast to the exposure to dry oxygen when the Xe marker did not move during exposure [20]. Hultquist et al. [16] indicated that the oxidation rate decreases if a better balance between Zr ion and oxygen ion transport is obtained, resulting in adherent oxide growth, with low density of pores and other defects.

In this paper, the effect of deuterium (D) and the combined effect of Pt and deuterium (D) on the oxidation of Zr at 400 °C in 20 mbar O_2 are investigated. This is done by oxidation of partly Pt coated Zr samples with 600 wtppm D and without D, respectively. Finally, experiments where Ar-filled Zr-based tubes with ZrSn liner are exposed to water from one end of the tubings are presented. The results show that the deuterium (D) concentration in the oxide and substrate of two Zr-based tubes varies as well as the oxide thickness upon exposure in H_2O/D_2O at 370 °C.

2. Experimental

2.1. Gas phase analysis (GPA) technique

The schematic diagram of the GPA equipment presented in Fig. 1 consists of:

- A 70 cm^3 reaction chamber made of a silica tube and a stainless steel cross. The reaction chamber is pumped with an ion pump via a leak valve. In oxidation test of the 1 m long Zr-based tubes, the silica tube in Fig. 1 is replaced by the Zr-based tube.
- A gas handling system where pressures up to 1 atm can be used.
- A pressure gauge to measure the total pressure inside the reaction chamber.
- A mass spectrometer (MS), with a quadruple analyser, placed in an UHV chamber. Hydrogen and different isotopes can be detected.
- A tube furnace which can be used up to 1200 °C.

The GPA equipment can be used for different types of measurements: outgassing, hydration, oxidation, dissociation and exchange. These different measurements are shortly described bellow with some examples.

2.1.1. Outgassing

Heating of a sample in vacuum generates release of gases that can be quantified with a relevant calibration. This enables, for example, the hydrogen content in a material to be determined. In Fig. 2, the outgassing of hydrogen from a Zr plate at temperatures up to 700 °C is shown. The outgassing method has previously been described in detail [21].

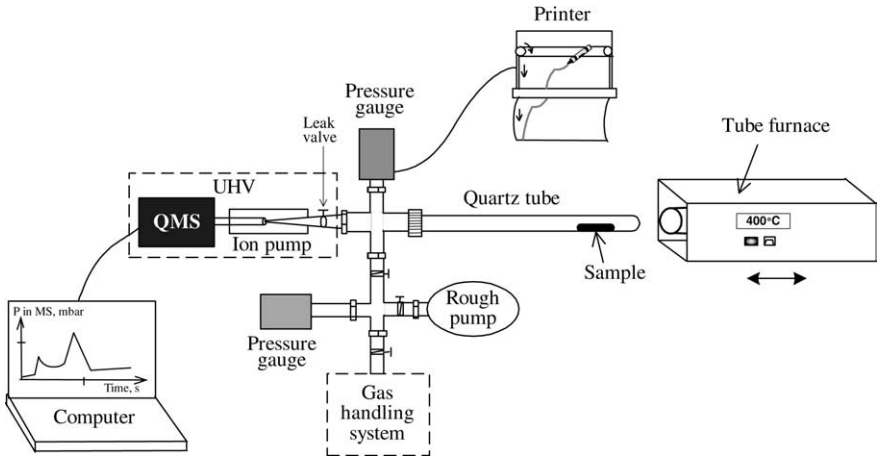

Fig. 1. GPA equipment for outgassing, hydration, oxidation, dissociation and exchange experiments.

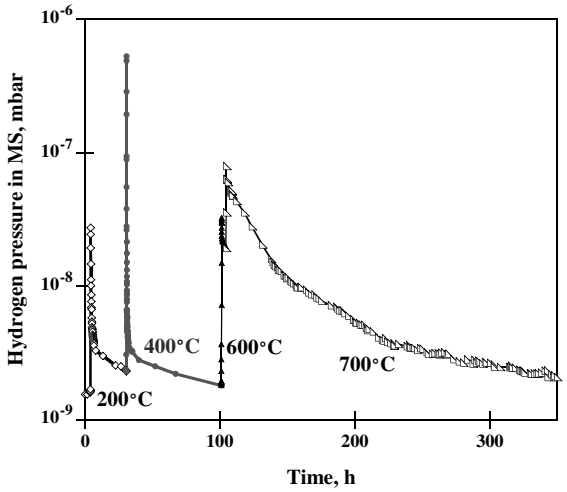

Fig. 2. Outgassing of hydrogen from a Zr-plate at temperatures up to 700 °C.

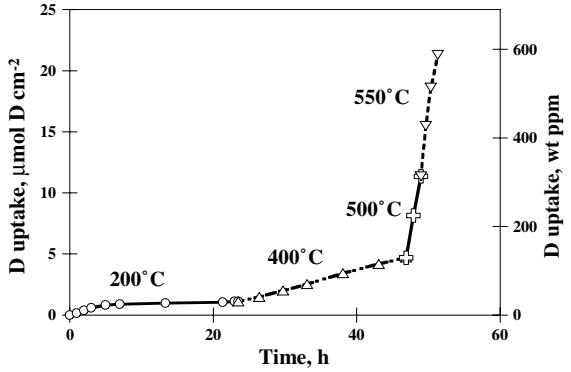

Fig. 3. Kinetics of deuterium (D) uptake in a Zr plate.

2.1.2. Hydration and oxidation

The most common way to study oxidation of metals is measurement of the weight gain of the sample. With GPA, the changes in the gas phase are measured. The pressure decrease of the gas in the reaction chamber upon time is continuously monitored and is conveniently recorded on an x–t plotter. A 1.8 cm^2 Zr plate covered with a naturally formed oxide was exposed to 7.5 mbar deuterium (D) at temperatures 200–550 °C. Calculated from the decrease of D_2-pressure in the reaction chamber, the deuterium (D) uptake versus time in the Zr plate is shown in Fig. 3. After charging, the D content in the Zr plates was 600 wtppm. As seen in the figure, the uptake rate of D in Zr is increasing considerably at temperatures above 400 °C.

For study of the oxidation mechanism, the oxidation can be performed in two stages, first in 'normal' O_2 followed by exposure in ^{18}O-enriched O_2. In a subsequent analysis with SIMS the position of the oxide growth can be found if the exchange rate between O in the oxide and O in O_2 is slow compared with O-uptake rate in the oxidation. The previously D-charged Zr plate, labelled Zr(D), was partly coated with Pt and exposed at 400 °C for 12 h to 20 mbar O_2 in two stages. The oxidation kinetics presented as oxygen uptake from the gas phase is shown in Fig. 4. (SIMS profiles of the reaction products are presented in the results section of the paper.)

2.1.3. Dissociation and exchange measurements

The interaction between gas molecules and a surface can lead to dissociation (molecules split into smaller constituents). The surface activity of a material for dissociation can be quantified [22]. To measure the dissociation rate of a molecule, a mixture of its isotopes are used, e.g. $^{16,16}O_2 + {}^{18,18}O_2$. The dissociation process

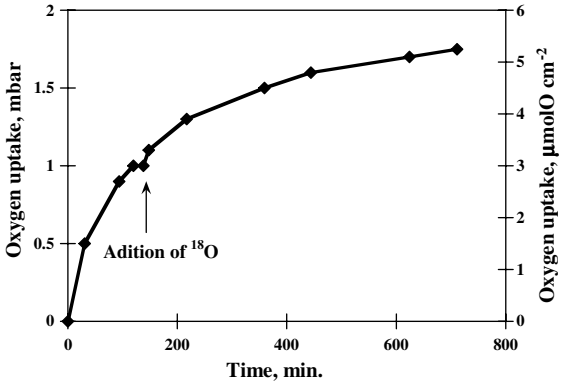

Fig. 4. Oxidation of a partly Pt coated Zr sample containing 600 wtppm D, Zr(D), in 20 mbar O_2 at 400 °C.

and a subsequent association of the dissociated species result in the formation of the mixed molecules $^{16,18}O_2$. The partial pressures of the gas components, $^{16,16}O_2$, $^{16,18}O_2$ and $^{18,18}O_2$, are obtained via an inlet to the MS. The inlet is small enough not to influence the total oxygen pressure in the reaction chamber. By considering the measured formation rate of the mixed molecules and the distance from the statistical equilibrium (no more changes in the gas composition), the dissociation rate can be calculated. The background dissociation rate of the silica tube must of course also be taken into account. A detailed description of the measurements has been presented elsewhere [22].

Exchange may take place between oxygen in the gas phase and oxygen in the oxide. This exchange can be measured in exposure of a ^{16}O-containing oxide to $^{18,18}O_2$. The formation rate of $^{16,18}O_2$ in the gas phase will then be a result of exchange between ^{18}O from the gas phase and ^{16}O from the oxide lattice.

2.2. Characterization of the exposed samples

In Table 1 samples and analysis methods used in this study are collected.

2.2.1. Secondary ion mass spectrometry analyses

SIMS analyses were performed with a Cameca IMS-6f apparatus, 10 keV, 50–200 nA primary beam of Cs^+ ions, which was rastered over 200×200 μm^2, where ions where detected from a centered area with a diameter of 70 μm.

2.2.2. X-ray photoelectron spectroscopy, XPS

After oxidation, the outermost layers on the Zr samples were analyzed with X-ray photoelectron spectroscopy, XPS, with Kratos AXIS HS. Detailed scans (pass energy of 80 eV) of C 1s, Zr 3d, O 1s, Pt 4f were obtained with a monochromatic AlKa(alfa) X-ray source (1486.6 eV). The area of analysis was approximately 0.4 mm^2. The binding energies for O 1s and Zr 3d were corrected related to C 1s peak (285 eV).

2.2.3. Scanning Electron Microscopy, SEM

FEG–SEM analysis was performed with a Leo 1530 Field Emission Scanning Electron Microscope equipped with a GEMINI field emission column.

3. Results and discussion

3.1. Oxygen dissociation on Zr-based materials and Pt

Westinghouse Electric Sweden AB has supplied Zircaloy-2 and Zr_2Fe, Zr_2Ni, $ZrCr_2$-intermetallics used in this work.

Before dissociation experiments, Zr_2Fe, Zr_2Ni, $ZrCr_2$ intermetallics have been oxidized for 80 min in approxi-

Table 1
Samples, analysis methods with respective figure numbers

Sample	Hydrogen content	Pt coating	Temperature (°C)	Analysis methods				Figure
				GPA	SEM	SIMS	XPS	
Oxygen dissociation measurements								
Zr_2Fe	<5 wtppm H	No	400	×				5, 6
Zr_2Ni	<5 wtppm H	No	400	×				5, 6
$ZrCr_2$	<5 wtppm H	No	400	×				5, 6
Zircaloy-2 plate	<5 wtppm H	No	500–700	×				5, 6
Pt plate	–	–	400–700	×				5, 6
Pt and D influence on Zr oxidation								
Zr(D) plate	<1 wtppmH + 600 wtppm D	Yes	400	×		×	×	3, 4, 7, 9–14
Zr plate	<5 wtppm hydrogen	Yes	400	×	×	×	×	7–10, 12–14
Oxidation of Zr-based tubes in water								
Zr-based tube 1 (inside)	<1 wtppm H	No	370	×		×		15, 16
Zr-based tube 2 (inside)	<1 wtppm H	No	370	×		×		15–17

mately 65 mbar $^{16,16}O_2$ at 400 °C resulting in 19, 0.8 and 0.4 μm oxide thickness respectively. Zircaloy-2 was oxidized for 90 h in approximately 200 mbar $^{16,16}O_2$ at 400–500 °C resulting in 2.5 μm oxide thickness.

In Fig. 5, the formation rate of the mixed oxygen molecules, $^{16,18}O_2$, during the exposure of a 2 cm^2 pre-oxidized Zr_2Fe intermetallic sample at 400 °C and a 28 cm^2 pre-oxidized Zircaloy-2 sample at 500 °C to approximately 50% ^{18}O-containing oxygen gas mixture are presented. Though at lower temperature, and with a much smaller surface area, the formation rate of the mixed molecules is higher on the Zr_2Fe sample. This implies that the Zr_2Fe has a considerably higher oxygen dissociation efficiency than Zircaloy-2.

Oxygen dissociation rate on Pt as well as on pre-oxidized Zr_2Fe, Zr_2Ni, $ZrCr_2$ and Zircaloy-2 in exposure to 20 mbar O_2 has been measured and the results are summarized in Fig. 6. At temperatures around 400 °C, oxygen dissociation efficiency is decreasing in the order Pt > Zr_2Fe > Zr_2Ni > $ZrCr_2$ ⩾ Zircaloy-2. (The accuracy in the measurement of $ZrCr_2$ sample only allowed us to determine the dissociation rate of O_2 on $ZrCr_2$ to be lower than 2×10^{-12} mol O cm^{-2} s^{-1}.)

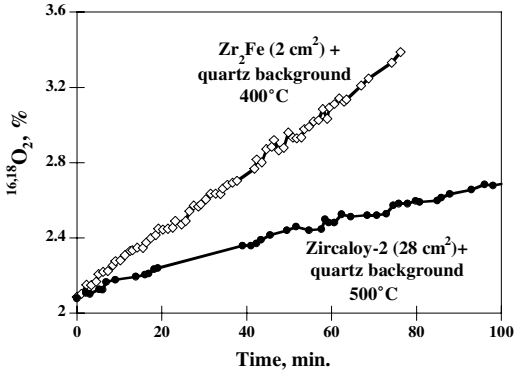

Fig. 5. Oxygen dissociation measurements on Zr_2Fe and Zircaloy-2.

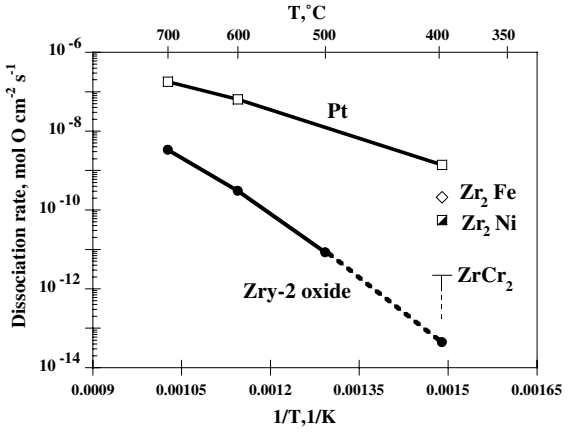

Fig. 6. Oxygen dissociation rates on Pt as well as pre-oxidized Zr_2Fe, Zr_2Ni, $ZrCr_2$ and Zircaloy-2 in exposure to 20 mbar O_2 versus reciprocal temperature. The value of oxygen dissociation at 400 °C on pre-oxidized Zircaloy-2 is extrapolated.

Fe, Cr and Ni have a low solubility in the Zr matrix and are therefore mainly incorporated in the form of SPP [8,23] and also partly incorporated in the oxide during oxidation. The size distribution of SPPs in the Zr-based materials has an important effect on the in-reactor performance of these materials [23]. The formation rate of protective oxides and also the thickness of the barrier layer are found to be dependent on the initial SPP size distribution [23]. Dissolution of small-size SPPs in Zr-based materials during in-reactor operation under high neutron flux in combination with hydrogen pick-up can enhance the deterioration of the barrier layer [23].

The chemical composition of SPPs is also important [23]. In Zircaloy-2, for example, two types of SPPs are reported: $Zr_2(Fe,Ni)$ and $Zr(Fe,Cr)_2$ particles [3,8,23,24]. The Cr-containing particles were found to be less resistant to dissolution in the matrix during irradiation than the Ni-containing particles [3,23]. Each alloying element has certain effects on the oxidation and it seems plausible that one effect is related to efficiency for oxygen dissociation. Thus the results from Fig. 6 suggest that among Zr_2Fe, Zr_2Ni and $ZrCr_2$, the Fe-containing particles are the most effective in dissociation of O_2 at 400 °C. It is reported that the addition of up to 150 ppm Fe to pure Zr is beneficial for the corrosion resistance [24]. Our suggested explanation for this observation is linked to a synergistic effect of oxygen dissociating elements, such as Fe, and hydrogen and is discussed in the section below.

3.2. Influence of Pt and deuterium on the oxidation of Zr in O_2 at 400 °C

Two 1.8 cm^2 Zr plates were outgassed at temperatures up to 700 °C (Fig. 2). The hydrogen content in the samples after outgassing was less than 5 wtppm. One sample was charged with deuterium to 600 wtppm D (see Fig. 3). Both samples were then partly sputter-coated with 200 Å porous Pt.

The samples were placed in the GPA equipment and the reaction chamber was evacuated at temperatures up to 400 °C for 12 h. Oxidation was carried out in two stages at 400 °C. First in $^{16,16}O_2$ then in ^{18}O-enriched oxygen gas (85% ^{18}O for Zr(D) sample and 52% ^{18}O for Zr sample) for totally 12 h exposure to approximately 20 mbar gas. The experimental conditions are summarized in Table 2 and the samples are shown in Fig. 7. The oxygen uptake from the gas phase was used to calculate the average oxide thickness in the oxidation. In 12 h of oxidation a 0.6 μm oxide was formed on the D-containing sample (see Fig. 4 for oxygen uptake rate)

Table 2
Experimental conditions for the oxidation of Zr(D) and Zr samples

Sample	Hydrogen content	Gas phase composition in oxidation, % (oxidation time)		Average oxide thickness[a], μm
		First stage	Second stage	
Zr(D)	<1 wtppm H + 600 wtppm D	99.9% ^{16}O (130 min)	85% ^{18}O + 15% ^{16}O (590 min)	0.6
Zr	<5 wtppm hydrogen	99.9% ^{16}O (130 min)	52% ^{18}O + 48% ^{16}O (590 min)	0.8

[a] For conversion an average density of 6 g cm^{-3} was considered for the oxide.

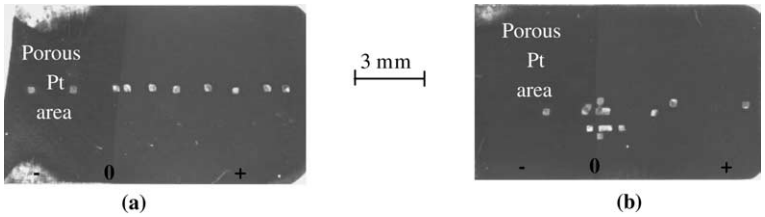

Fig. 7. Partly Pt coated Zr samples with visible craters from SIMS sputtering: (a) Zr(D) sample and (b) Zr sample.

whereas a 0.8 μm oxide was formed on the D-free sample.

After oxidation, the samples were characterized with SIMS, XPS, SEM and optical microscopy. In Fig. 8, SEM images of the area with Pt particles before and after oxidation of the Zr sample are shown.

3.2.1. SIMS results – oxygen transport in oxide

SIMS depth profiles (SIMS analysis points seen in Fig. 7) and XPS were used to characterize the oxide on areas with Pt particles and at different distances from the Pt area.

In Fig. 9, the SIMS integrated oxygen count rates from the second stage of oxidation are presented for the two Zr samples. Obviously in the Pt-area a considerably higher oxidation rate has taken place. A possible reason is that in the Pt area, oxygen dissociates on the Pt particles with high efficiency (see Fig. 6). The O^{n-} ($n = 0, 2$) species resulted from dissociation can then:

- associate and form molecular O_2,
- diffuse laterally via surface diffusion,
- diffuse through the oxide layer to the O/M interface.

In the Pt area, the lateral diffusion length corresponds to the distance between the Pt particles, which is 10–20 nm as can be seen in Fig. 8. In the Pt area, the O^{n-} concentration is high at the O/G interface, with a high concentration gradient of O^{n-} over the oxide thickness and therefore facilitating a high inward oxygen flux. At the interface between the area with Pt-particles and area without Pt-particles, the oxygen dissociation rate decreases about 10^5 times as can be seen in Fig. 6. Especially for the D-containing sample, a mm-ranged effect of Pt is observed in Fig. 9.

In the Pt area, high oxidation rates by inward oxygen transport generate thick oxides with defects, which also may enhance molecular transport. The thinnest oxide is found near the Pt area on the Zr(D) sample in Fig. 9. A local minimum in the oxygen uptake can also be found near the Pt area on the Zr sample. These observations suggest that in the vicinity of Pt area, which has a lower activity of O^{n-} compared with the Pt area, an outward Zr diffusion induced by D from the substrate balances the O^{n-} inward flux. The balanced growth facilitates a self-repairing mechanism to be operative and can explain the formation of a more dense oxide. At all positions the oxide on the Zr(D) sample is thinner than at corresponding positions on the Zr sample. This can be seen as a combined effect of Pt and D on Zr oxidation. Exchange between ^{18}O from the gas phase and ^{16}O from the oxide formed in the first stage is almost negligible at 400 °C.

To compare the oxidation mechanism inside the Pt area and far away from the Pt area, SIMS profiles of $Zr^{18}O$ and $Zr^{16}O + Zr^{18}O$ are considered and presented in Fig. 10(a) and (b) where also Pt count rates are shown.

The oxidation mechanism can be retrieved by considering the $Zr^{18}O$ SIMS profiles (oxidation in ^{18}O containing gas mixture was carried out in the second stage). High $Zr^{18}O$ count rates indicate where oxide growth mainly takes place. As clearly seen in Fig. 10, in the Pt area on both samples an enhanced oxidation takes place mainly by inward oxygen transport. Pt is enriched at the O/G interface.

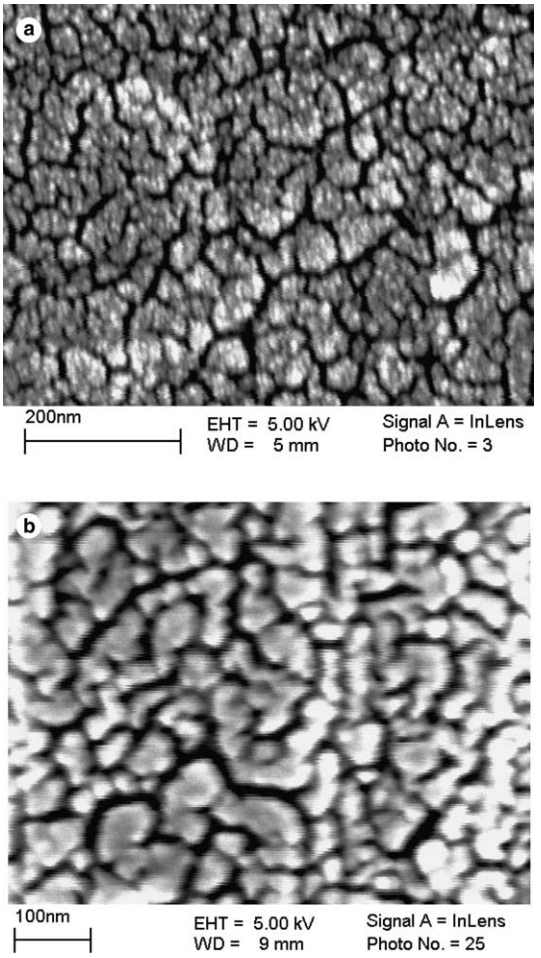

Fig. 8. SEM images of the area with Pt particles on Zr substrate: (a) before oxidation and (b) after 12 h oxidation in O_2 at 400 °C.

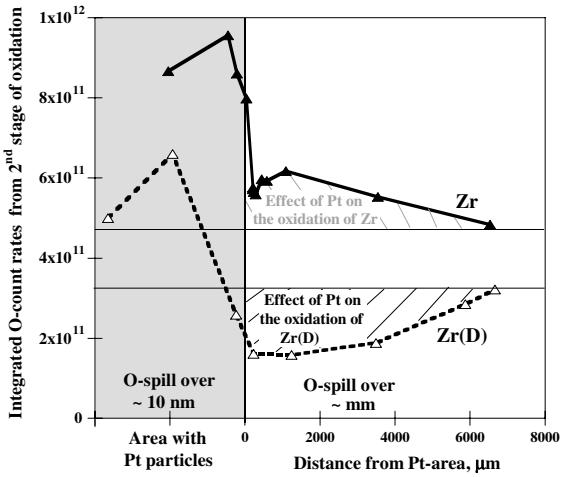

Fig. 9. SIMS integrated oxygen count rates from second stage of oxidation on different positions on the two samples after two-stage oxidation at 400 °C.

Relatively high $Zr^{18}O$ count rates are found for the Zr(D) sample far away from the Pt area at the O/G interface, which could be related to a D-induced outward Zr diffusion.

3.2.2. SIMS results – hydrogen transport

The SIMS profiles of deuterium (D) for the Zr(D) sample in different positions from the Pt area, after 12 h oxidation are shown in Fig. 11. In this figure, arrows indicate the position of the O/M interface based on sputter time when the ^{90}Zr ion count rate has decreased to half of its maximum value.

The area close to the O/G interface is magnified in Fig. 11 to show the difference between the D maxima at different distance from Pt area. For all positions except in the Pt area a local maximum appears near the O/G interface. This can result from a suppressed D outward diffusion in the Pt area. A local maximum in the D count rate appears also near the O/M interface at all analyzed positions. D outward transport is slightly increasing as the distance from the Pt area increases. The highest concentration of D in the oxide is found at the longest distance away from the Pt area, +6662 μm.

It is reported in the literature [25] that hydrogen atoms dissolved in the Zr substrate prefer tetrahedral interstitial sites and they diffuse interstitially. The radius of these tetrahedral interstitial sites is approximately 0.036 nm [25]. The radius of hydrogen atom is about 0.04 nm [25], which means that the strain induced by hydrogen dissolution in Zr is negligible [25]. Zhang et al. [25] have found that hydrogen tends to segregate to the Zr surface. When dissolved oxygen is present in the Zr substrate, hydrogen segregation to the Zr surface is enhanced [25]. The concentration of dissolved oxygen in Zr varies from the bulk to the surface and is much higher underneath the oxide, accommodating also more hydrogen in this area.

In our Zr samples, prior to oxidation the hydrogen content was <5 wtppm H and (<1 wtppm H + 600 wtppm D) respectively. SIMS profiles of H, D and (H + D) are presented in Fig. 12 for the two Zr samples at +3543 μm, Zr, and +5871 μm, Zr(D), away from respective Pt area. From Figs. 11 and 12 it is observed that:

- A high H concentration appears at the G/O interface, which is likely due to 'contamination' and/or ^1H SIMS background.
- D contamination is negligible at the G/O interface, which indicate that accurate information requires the use of D instead of H.

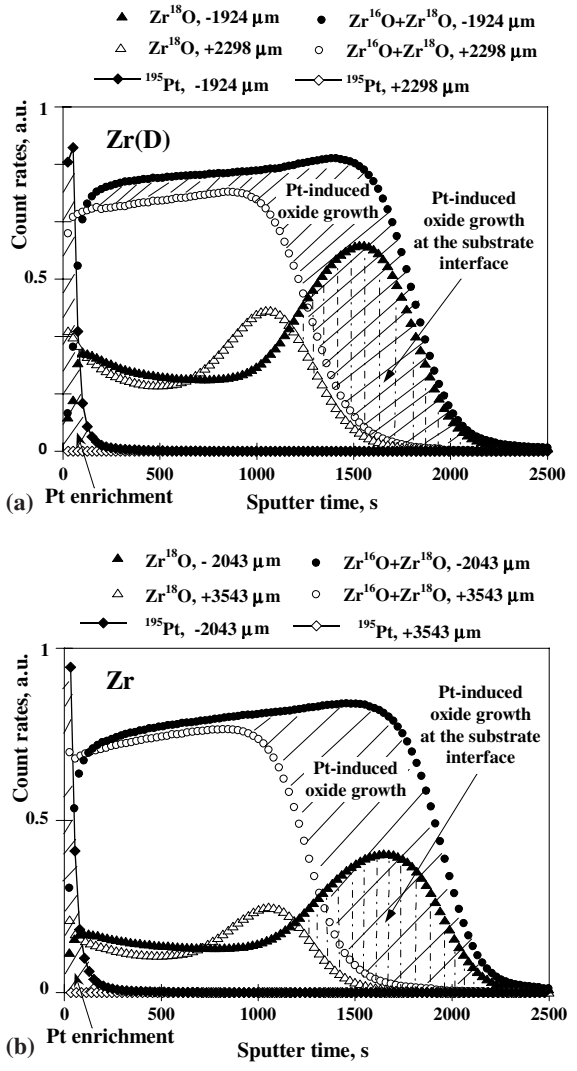

Fig. 10. SIMS depth profiles inside Pt area (–) and far away from Pt area (+) for (a) Zr(D) sample and (b) Zr sample.

- The ^{1}H SIMS depth profile on the sample with <5 wtppm H shows a maximum inside the metal at the O/M interface but no corresponding maximum is found on the sample with <1 wtppm H + 600 wtppm D.
- The D profile shows a local maximum inside the oxide, near the O/M interface at all analyzed positions. As going away from the Pt area, a small but increasing accumulation of D appears at the G/O interface.

Stern et al. [26] have reported that a maximum in hydrogen concentration is obtained in the metal region immediately under the oxide after oxidation of pre-hydrated Zr-based materials. They suggested that an interaction between the interstitially dissolved H (occupying the tetrahedral sites) and O (occupying the octahedral sites) under the oxide layer is responsible for these sub-oxide peaks in the hydrogen profile. However the peak in D in our experiments is located in the oxide near the O/M interface and this fact is further considered below.

(a) Hydrogen concentration in the Zr substrate is low and is close to the dissolved oxygen concentration in the metal region immediately under the oxide ($C_H \approx C_O$). H from the substrate is diffusing from the bulk to the surface during oxidation and short range bonds between dissolved O and H can take place at the O/M interface. This results in a maximum in the H profile in the metal region immediately under the oxide.

(b) Hydrogen concentration in the Zr substrate is high and greatly exceeds the dissolved oxygen concentration in the metal region immediately under the oxide ($C_H \gg C_O$). A small fraction of the outward diffusing H from the bulk will be trapped in short-range bonds with the dissolved O, but a main part will diffuse into the oxide where it can be accommodated in tetrahedral sites [27]. This can explain the maximum that appears in the oxide near the O/M interface on the sample with 600 wtppm D in the substrate.

It is reported that in zirconia, protons are not centred in a normal interstitial position but are closely bonded to oxygen ions [27]. The 'substitutional hydroxide' term is frequently used to refer to this defect [27]. The presence of hydrogen in zirconia influences the bonds of the neighbouring atoms, Zr and O. We suggest that in the oxidation of Zr-based materials in water containing atmospheres, hydrogen accumulation in the oxide near the O/M interface could explain the frequently observed deterioration of the 'barrier' layer. This also indicates that Zr could move easier in the deteriorated barrier when hydrogen is present. Partially 'degraded' oxide within the barrier layer due to hydrogen was also considered by Elmoselhi [28], in the exposure of a pre-oxidized Zircaloy-2 to a low pressure of deuterium (D) at 380 °C for 15 days.

In our case, for the Zr(D) sample in the Pt area, the enhanced oxygen inward transport can also generate more dissolved oxygen, which can trap more deuterium (D). The outward transport of deuterium (D) to the G/O interface is also lowered due to the longer diffusion length (thicker oxide) obtained in the Pt area.

Deuterides are expected to be present in the Zr(D) sample, the D content being above the solubility limit. It is reported [7] that the thermal solid solubility (TSS) of H in Zr at 400 °C is approximately 200 wtppm H.

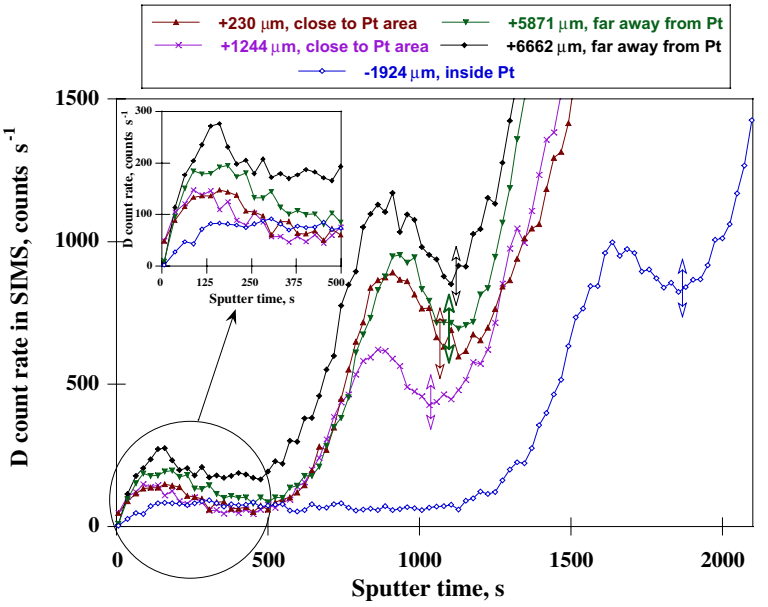

Fig. 11. SIMS depth profiles of D at different positions on the Zr(D) sample after oxidation. The oxide/metal interface is indicated by arrows.

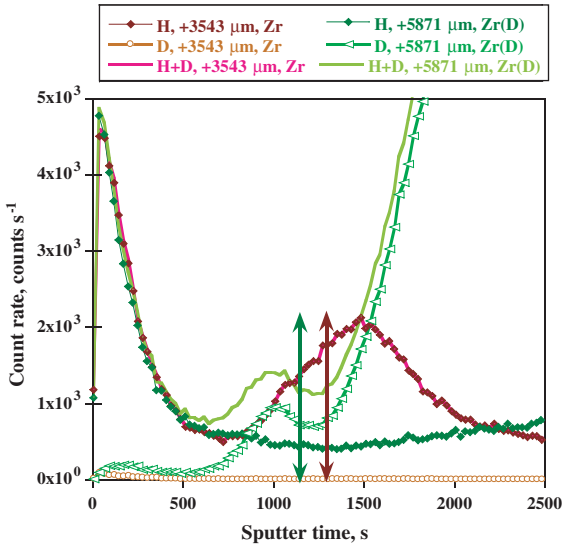

Fig. 12. H and D SIMS depth profiles far away from the Pt area for the two Zr samples after 12 h oxidation in 20 mbar O_2 at 400 °C. The arrows indicate the oxide/metal interface (grey (green) for Zr(D) sample and black (red) for Zr sample). Profiles of H and (H + D) for Zr sample virtually coincide. For interpretation of the references to colour the reader is referred to the web version of this article.

Analysis of the ^{18}OD and D SIMS profiles away from Pt area, shown in Fig. 13, are considered to elucidate the connection between deuterium (D) and oxygen during Zr oxidation. The sample without D is also shown in

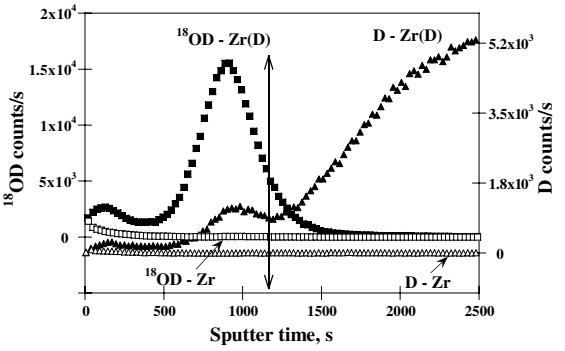

Fig. 13. SIMS ^{18}OD and D count rates for the Zr samples after oxidation in 20 mbar O_2 at 400 °C far away from the Pt area (+6662 μm from the Pt area for Zr(D) sample and respectively +6534 μm from the Pt area for Zr sample). The arrow indicates the position of the oxide/metal interface.

Fig. 13 for comparison of ^{18}OD and D count rates. The O/M interface for Zr(D) sample is indicated in the figure. Close to this interface, a distinct maximum in ^{18}OD can be seen as well as a local maximum in D which may confirm formation of 'substitutional hydroxides' in the oxide close to the O/M interface.

3.2.3. XPS results

XPS was used to characterize the outermost oxide layer at different positions from the Pt area.

In Fig. 14, the O 1s and Zr $3d_{5/2}$ binding energies are shown for different distance from the Pt area. The

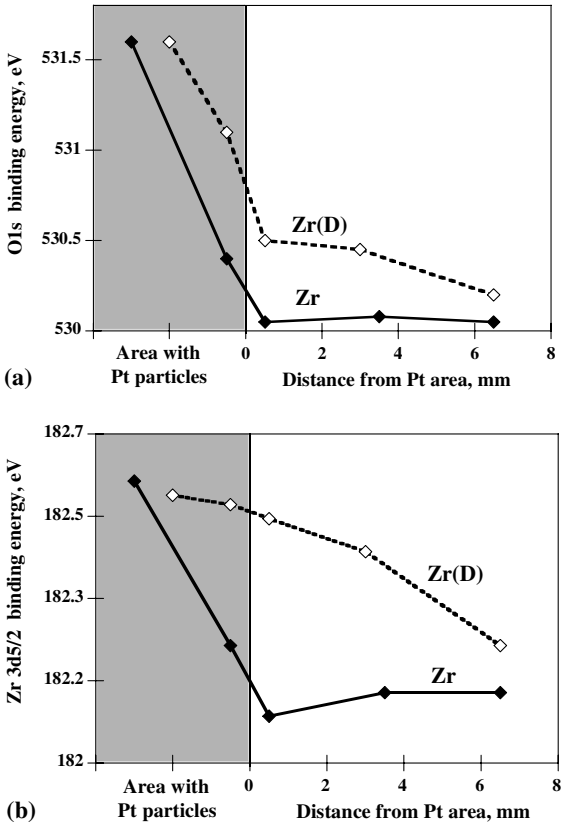

Fig. 14. XPS analysis: (a) O 1s binding energy and (b) Zr 3d 5/2 binding energy, at different positions on the two samples. The C 1s was set to 285 eV, which was used as an internal reference.

binding energies were corrected related to C 1s peak (285 eV). Comparing the area with and without Pt particles, a chemical shift in the O 1s binding energy of approximately 1.5 eV is obtained for both Zr samples. For both samples, the O 1s binding energy inside Pt area has the highest value of 531.6 eV. The deuterium (D) is not influencing the O 1s binding energy in the Pt area significantly, as indicated previously since D outward diffusion at the G/O interface is suppressed in this area. Away from the Pt area, the change in O 1s binding energy is more pronounced for the Zr(D) sample. The Zr $3d_{5/2}$ binding energy in Fig. 14(b) on the Zr(D) sample is rather different from the Zr sample.

The formation of Zr suboxides was investigated by Nishino et al. [29] in the initial oxidation stages of Zr and Zircaloy-2 with oxygen and water vapor at room temperature using Auger and X-ray photoelectron spectroscopy. The binding energy values for Zr $3d_{5/2}$ used in their study [29] were for Zr in ZrO_2, 182.9 eV and for Zr in Zr_2O_3, 181.8 eV. Our values are ranging from 182.1 eV close to Pt area to 182.6 eV inside Pt area for the Zr sample. It seems plausible that at the O/G interface, the Zr oxidation state varies, being high in the Pt area (probably ZrO_2 or ZrO_{2+x}), and some suboxides are probably present away from the Pt area. The presence of D in the Zr(D) sample generates higher binding energies for O 1s and Zr $3d_{5/2}$, especially outside Pt area, possibly due to the presence of D at the G/O interface.

3.3. Oxidation of Zr-based tubes in water at 370 °C

Two Zr-based tubes with ZrSn liner were used in experiments where the tubes were Ar-filled and, subsequently, exposed to water from one end of the tubings. The experimental set-up is schematically shown in Fig. 15. The tubes were evacuated for 24 h at 370 °C before exposure and then filled at 370 °C with approximately 700 mbar Ar and exposed from one end to an inlet of approximately 22 mbar H_2O for 305 min (first tube) and 22 mbar D_2O for 630 min (second tube).

After exposure, the tubes were visually inspected. The oxide thickness had a local minimum at a certain distance from the water inlet. This was observed in both tubes but at slightly different distances from the water inlet. SIMS analyses at different positions from the water inlet were used to characterize the oxide thickness and the hydrogen content after oxidation of the tubes.

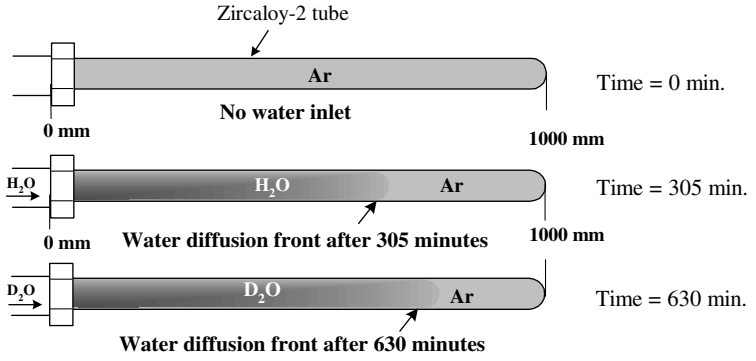

Fig. 15. Experimental set-up for the exposure of Ar-filled Zircaloy-2 tubes with ZrSn liner to 22 mbar H_2O (D_2O) at 370 °C.

Integrated SIMS count rates of oxygen and deuterium (D) along the length of the tubes are shown in Fig. 16. Thickest oxide was obtained at 330–400 mm from the water inlet. Local minima in the oxide thickness are found at 430 mm and 478 mm respectively from the water inlet. At these positions there is some hydrogen in the substrate as a result of the reaction with water. In this case, both oxygen and hydrogen diffuse inward towards the O/M interface. At 996 mm from the water inlet position no significant oxidation takes place but the deuterium (D) content is slightly higher than at the water inlet position (20 °C). Deuterium (D), resulted from the reaction of D_2O with Zr at 370 °C, diffuses faster than D_2O through the Ar filled tubes. The deuterium (D) concentration underneath the oxide in the second tube is presented in Fig. 17. In the area where the oxide is thickest, around 330 mm from the water inlet, the concentration of deuterium (D) underneath the oxide is the

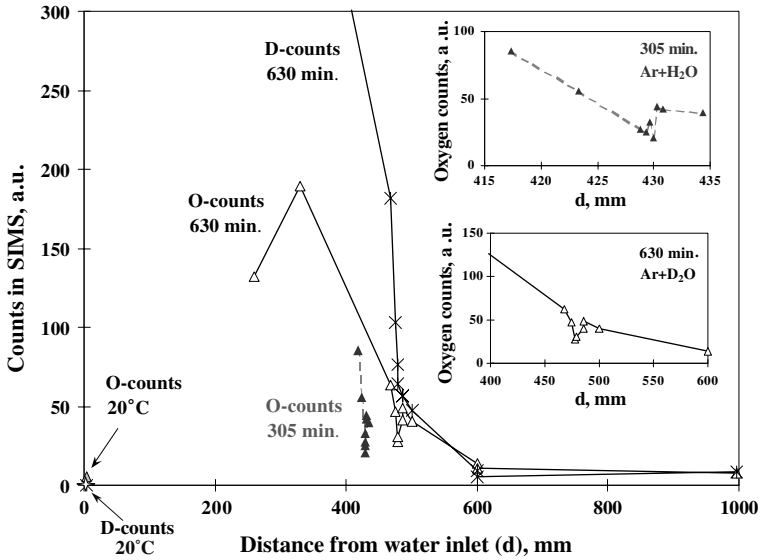

Fig. 16. SIMS analysis of the Zr-based tubes: integrated oxygen and deuterium (D) count rates at different positions from the water inlet.

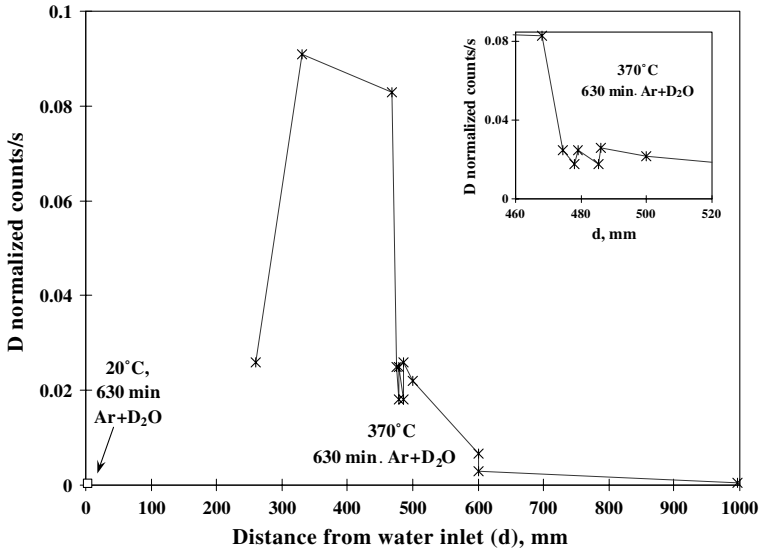

Fig. 17. SIMS analysis of the Zr-based tubes: deuterium (D) count rate in the metal underneath the oxide versus position in tube. In the range 260 → 1000 mm the tube temperature is approximately 370 °C.

highest. There is a tendency for local minima in the D content at positions close to 478 mm from the D_2O inlet.

The experiment shows that the hydrogen content in the substrate influences the formation of the oxide layer. After starting the oxidation but before water reaches to 430 mm (tube 1) and respectively 478 mm (tube 2) from the water inlet position, the D content in the substrate in these positions increases. At 370 °C, the oxide formed at these positions is denser, being characterized by a slow oxygen and deuterium (D) diffusion. We suggest that a certain amount of hydrogen seems to be beneficial for the formation of dense Zr-oxide. This may be understood by a more balanced O/Zr transport, where the Zr-transport is induced by hydrogen.

3.4. Interpretation of the experimental results

In oxidation of Zr-based materials, the oxide growth takes place mainly by inward oxygen transport, which creates a network of micropores, or rather nano-pores. These pores can easily act as diffusion paths for molecular species. Hydrogen present in the substrate or in the corrosive environment diffuses in the oxide layer and tends to generate deterioration of the barrier layer. However, hydrogen also generates outward diffusing Zr, which can react with oxygen or water molecules within the oxide and/or at the G/O interface. Obviously healing of pores by oxide formation needs outward Zr transport.

In the case of inward hydrogen transport (Fig. 17), the area where the oxide thickness shows a local minimum, the D content underneath the oxide is relatively low. By blocking the molecular diffusion pathways, relatively more ionic transport pathways are used for the transport of species through the oxide layer, which is a slower transport near 400 °C, resulting in growth of more protective and thinner oxides. Related to the 'self repairing' concept, a small but significant fraction of Zr outward diffusion was identified in the 600 wtppm D containing Zr sample in oxidation in dry O_2 at 400 °C.

4. Summary

The transport of oxygen and hydrogen through the growing zirconia layer in the oxidation of Zr-based materials in O_2 at 400 °C and in water at 370 °C is investigated using gas phase analysis (GPA) and secondary ion mass spectroscopy (SIMS).

4.1. Oxygen dissociation on Zr-based materials and Pt

- The dissociation rate of the O_2 on pre-oxidized-Zr_2Fe is considerably higher than on pre-oxidized-Zircaloy-2 at 400 °C.
- At temperatures around 400 °C, oxygen dissociation efficiency decreases in the following order: $Pt > Zr_2Fe > Zr_2Ni > ZrCr_2 \geqslant$ Zircaloy-2.

4.2. Influence of Pt and deuterium on the oxidation of Zr in O_2 at 400 °C

The influence of Pt on the oxidation of Zr, with and respectively without D in the substrate, at 400 °C in dry O_2 was investigated. After oxidation, the samples were characterized with SIMS, XPS, SEM and optical microscopy.

4.2.1. SIMS results

- An enhanced oxidation rate is observed in the Pt area for both samples. The deuterium (D) outward diffusion is suppressed in the Pt area.
- In the vicinity of the Pt area a local minimum in oxide thickness is obtained for both samples and thinnest oxide is obtained on the Zr(D) sample.
- At areas away from the Pt area, the D SIMS depth-profile shows a maximum at the G/O interface, which is more pronounced as the distance from the Pt area increases.

The formation of 'substitutional hydroxides' at the O/M interface is proposed as a mechanism for oxide deterioration. Hydrogen may also induce Zr diffusion in the oxide, resulting in new oxide formation with fewer defects. If the hydrogen content is high the dissolution rate may become higher than the healing capacity by oxide growth within the oxide and lead to deterioration of the oxide.

4.2.2. XPS results

The XPS results reveal that Zr has different oxidation states in the oxides formed in the Pt area and outside Pt area. A high oxidation state is obtained in the Pt area.

4.3. Oxidation of Zr-based tubes in water at 370 °C

The exposure of two Ar-filled 1 m long Zircaloy-2 tubes with ZrSn liner to 22 mbar water at 370 °C for 305 and respectively 630 min was investigated. The oxide thickness and the hydrogen content were measured at different positions from the water inlet using SIMS depth profiles.

Local minima in oxide thickness are obtained at 430 mm and respectively 478 mm from the water inlet. Hydrogen gas produced in the oxidation reaction is diffusing 'ahead of the steam front' and is taken up by the tube material. The two positions corresponding to local minima in oxide thickness have a certain amount of hydrogen present in the substrate before being oxidized

by water. The D content underneath the oxide shows also that D uptake is small where the oxidation rate is low.

4.4. Main result

For a content of 600 wtppm D in the Zr substrate, a beneficial effect of Pt (high efficiency in oxygen dissociation) on the Zr oxidation in O_2 at 400 °C is found. Considering the O_2 dissociation efficiency at 400 °C on Pt and Zr_2Fe, we believe that an analogue beneficial effect of Fe-containing SPPs is operative when the chemical composition, size distribution and volume fraction of SPPs harmonize with the hydrogen concentration. We suggest that H-induced Zr outward diffusion is beneficial for healing defects like pores and microcracks formed in the oxide during oxidation. The formation rates of these defects, generated by an exclusive inward oxygen transport, can be counter battled by healing generated by outward Zr diffusion.

Acknowledgments

Financial support from Westinghouse Electric Sweden AB is gratefully acknowledged.

References

[1] E.A. Gulbransen, K.F. Andrew, J. Metals (1957) 394.
[2] B. Cox, Y.-M. Wong, J. Nucl. Mater. 218 (1995) 324.
[3] P. Rudling, G. Wikmark, J. Nucl. Mater. 265 (1999) 44.
[4] S. Abolhasssani, M. Dadras, M. Leboeuf, D. Gavillet, J. Nucl. Mater. 321 (2003) 70.
[5] A. Yilmazbayhan, A.T. Motta, R.J. Comstock, G.P. Sabol, B. Lai, Z. Cai, J. Nucl. Mater. 324 (2004) 6.
[6] B.H. Lim, H.S. Hong, K.S. Lee, J. Nucl. Mater. 312 (2003) 134.
[7] M. Oskarsson, E. Ahlberg, U. Södervall, U. Andersson, K. Pettersson, J. Nucl. Mater. 298 (2001) 315.
[8] C. Lemaignan, in: Zirconium in the Nuclear Industry: Thirteenth International Symposium, ASTM STP 1423, Annecy, France, 2001, p. 20.
[9] S.A. Raspopov, A.G. Gusakov, A.G. Voropayev, A.A. Vecher, M.L. Zheludkevich, O.A. Lukyanchenko, A.S. Gritsovets, V.K. Grishin, J. Chem. Soc. Faraday Trans. 93 (1997) 2113.
[10] X. Iltis, M. Viennot, D. David, D. Hertz, H. Michel, J. Nucl. Mater. 209 (1994) 180.
[11] N. Ramasubramanian, P. Billot, S. Yagnik, in: Zirconium in the Nuclear Industry: Thirteenth International Symposium, ASTM STP 1423, Annecy, France, 2001, p. 222.
[12] A.P. Zhilyaev, J.A. Szpunar, J. Nucl. Mater. 264 (1999) 327.
[13] P. Berger, R. El Tahhann, G. Moulin, M. Viennot, Nucl. Instrum. and Meth. B 210 (2003) 519.
[14] I.S. Woolsey, J.R. Morris, Corrosion 37 (1981) 575.
[15] I. Takagi, S. Shimada, D. Kawasaki, K. Higashi, J. Nucl. Sci. Tech. 39 (2002) 71.
[16] G. Hultquist, B. Tveten, E. Hörnlund, M. Limbäck, R. Haugsrud, Oxid. Met. 56 (2001) 313.
[17] B. Cox, Y.-M. Wong, J. Nucl. Mater. 270 (1999) 134.
[18] G. Hultquist, B. Tveten, E. Hörnlund, Oxid. Met. 54 (2000) 1.
[19] B. Tveten, G. Hultquist, T. Norby, Oxid. Met. 52 (1999) 221.
[20] A. Grandjean, Y. Serruys, J. Nucl. Mater. 273 (1999) 111.
[21] T. Åkermark, G. Hultquist, Q. Lu, J. Mater. Eng. Perf. 5 (1996) 516.
[22] E. Hörnlund, Appl. Surf. Sci. 199 (2002) 195.
[23] P. Tägtström, M. Limbäck, M. Dahlbäck, T. Andersson, H. Pettersson, in: Zirconium in the Nuclear Industry: Thirteenth International Symposium, ASTM STP 1423, Annecy, France, 2001, p. 96.
[24] P. Barberis, E. Ahlberg, N. Simic, D. Charquet, C. Lemaignan, G. Wikmark, M. Dahlbäck, M. Limbäck, P. Tägtström, B. Lehtinen, in: Zirconium in the Nuclear Industry: Thirteenth International Symposium, ASTM STP 1423, Annecy, France, 2001, p. 33.
[25] C.-S. Zhang, B. Li, P.R. Norton, J. Alloys Comp. 231 (1995) 354.
[26] A. Stern, D. Khatamian, T. Laursen, G.C. Weatherly, J.M. Perz, J. Nucl. Mater. 148 (1987) 257.
[27] T. Norby, in: S. Meriani, C. Palmonari (Eds.), Zirconia'88 – Advances in Zirconia Science and Technology, Elsevier Applied Science, London and New York, 1988, p. 209.
[28] M.B. Elmoselhi, J. Alloys Comp. 231 (1995) 716.
[29] Y. Nishino, A.R. Krauss, Y. Lin, D.M. Gruen, J. Nucl. Mater. 228 (1996) 346.